Journal Pre-proof

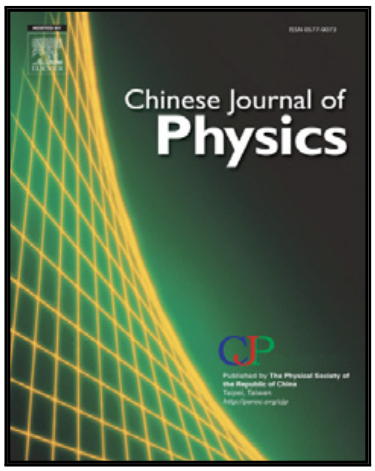

Heat generation/absorption effect on MHD flow of hybrid nanofluid over bidirectional exponential stretching/shrinking sheet

Nurul Amira Zainal , Roslinda Nazar , Kohilavani Naganthran , Ioan Pop

PII: S0577-9073(20)30316-6
DOI: https://doi.org/10.1016/j.cjph.2020.12.002
Reference: CJPH 1359

To appear in: *Chinese Journal of Physics*

Received date: 6 August 2020
Revised date: 29 November 2020
Accepted date: 1 December 2020

Please cite this article as: Nurul Amira Zainal , Roslinda Nazar , Kohilavani Naganthran , Ioan Pop , Heat generation/absorption effect on MHD flow of hybrid nanofluid over bidirectional exponential stretching/shrinking sheet, *Chinese Journal of Physics* (2020), doi: https://doi.org/10.1016/j.cjph.2020.12.002

- The boundary layer flow of a hybrid nanofluid near the stagnation-point is examined.
- The sheet is moving bidirectional exponentially.
- The fluid flow is under the effect of heat source/sink.
- The increment in the heat source descends the rate of heat transfer.
- Dual solutions are observable as the governing parameters vary.

Heat generation/absorption effect on MHD flow of hybrid nanofluid over bidirectional exponential stretching/shrinking sheet

Nurul Amira Zainal[a,b], Roslinda Nazar[a] , Kohilavani Naganthran[a*] and Ioan Pop[c].
[a]*Dept. of Mathematical Sciences, FST, UKM, 43600 Bangi, Selangor, Malaysia.*
[b]*FTKMP, UTeM, 76100, Melaka, Malaysia.*
[c]*Dept. of Mathematics, Babeş-Bolyai University, R-400084 Cluj-Napoca, Romania.*

[*]*Corresponding author*
Corresponding author's institutional email: kohi@ukm.edu.my
Corresponding author's telephone and fax numbers: +603-89213371 and +603-8925 4519

Abstract The idea of hybrid nanofluid has triggered many researchers because of its credential in improving the thermal characteristics. Hence, this study performed a mathematical analysis to evaluate the heat generation/absorption effect on magnetohydrodynamics (MHD) flow towards bidirectional exponential stretching/shrinking sheet of hybrid nanofluid. A system of ordinary differential equations was attained through a simplification of governing partial differential equations by employing appropriate similarity transformation and numerically determined via the bvp4c function in MATLAB programming system. The results revealed that the volume fraction of nanoparticle and magnetic parameter applied to the hybrid nanofluid improved the skin friction coefficient in the current work. The rate of heat transfer was strengthened by the intensity of the suction parameter, whereas the appearance of heat generation reduced the heat transfer rate performance. The results are proven to have dual solutions and lead to stability analysis implementation, hence confirming the first solution's achievability.

Keywords: Hybrid nanofluid, three-dimensional flow, stability analysis, MHD, heat generation/absorption

1. Introduction

The in-depth study of magnetohydrodynamics (MHD) flow phenomena is vital and has earned much attention owing to its significance practical applications in various industrial and engineering fields for instance, in fusion reactors, optical fibre filters, crystal growth, metal casting, optical grafting, and in the stretching of plastic sheets and metallurgical process ([1],[2]). The MHD involvement in an electrically conducting fluid results in resistive form force that yields motion resistance of the fluid particle, which can be defined as Lorentz force. The Lorentz force increases appreciably on the concentration and fluid temperature, therefore delaying the separation of the boundary layer. In 1974, the investigation over an electrically conducting liquid of the MHD boundary layer flow with a transverse magnetic field due to a stretching surface was first prompted by Pavlov [3]. In his notable study, a small magnetic Reynolds number was presumed, and from this standpoint, the induced magnetic field was disregarded. The work was broadened by Takhar et al. [4], who inspected the stability of the solution and reported that the magnetic field was discovered to have a stabilising effect on Taylor-Görtler three-dimensional disturbances. Since then, a considerable amount of reviews on MHD flow and heat transfer have been completed by many investigators, including the works in [5-8].

Many researchers and practitioners have strived to strengthen the analysis of heat transfer features and boundary layer characteristics past a stretching/shrinking sheet due to the overflowing purposes in the technology and manufacturing industry. Some of the industry applications are glass blowing, extrusion of plastic sheets, drawing plastic films, hot rolling, and so forth ([9],[10]). The end product quality of the desired features depends a lot on the heat transfer rate between the stretching/shrinking surface and fluid flow [11]. Sakiadis [12] pioneered the study of boundary layer flow over a moving continuous flat surface in constant speed by employing numerical solution and integral method supported by Crane [13] who

explored a two-dimensional laminar fluid flow in closed analytical form towards a linearly stretching sheet and successfully discovered the similarity solution in his findings. Magyari and Keller [14] were the first who introduced the study of boundary layer flow and heat transfer past an exponentially moving sheet. Soon after, many researchers have considered diverse aspects of this topic; for example, see [15-18]. In contrast, the study of a shrinking sheet (backward flow) has not captured much attention way back then due to its vorticity, which is not restrained within the boundary layer, and the flow is unlikely to occur unless a sufficient amount of suction is introduced on the boundary. Miklavčič and Wang [19] initiated the study of the shrinking sheet in a viscous flow and found non-uniqueness solutions. The characteristics of heat transfer and boundary layer examination towards the exponential shrinking surface was initially conducted by Bhattacharyya [20]. A substantial number of studies have been published in a persistence flow analysis over the exponentially stretching/shrinking sheet, including those of [21-25].

Over the years, nanotechnology development offers a remarkable transformation in our daily life. Numerous researchers have recently concentrated on this area because of its obvious significance in engineering and related fields. Choi and Eastman [26] were the earliest scholars who originated the nanofluid concept by illustrating the nanoparticle suspension in a base fluid. Nanofluids represents the class of colloidal mixtures (1–100nm) in a nanoparticle fluid suspensions that provide entry to the progressive growth of heat transfer mechanisms in nanotechnology [27],[28]. A critical analysis of the nanofluids' potential and achievement on the heat transfer enhancement has been extensively studied by academicians and scientists, for instance, see [29-33]. As nanofluids help researchers' quest for thermal efficiency, even today, a better form of working fluid is still in search. In coping with these, a higher-level type of nanofluids known as hybrid nanofluids is introduced, which believe may provide higher thermal

conductivity in contrast with nanofluids. This brand-new form of fluid agent has fascinated countless investigators because of its credential in developing and improving the thermal characteristics in real-life applications such as heat transfer devices in micro-channel, heat pipes, heat exchanger, air conditioning systems, and mini-channel heat sink [34-36]. An experimental analysis was set up by Madhesh and Kalaiselvam [37] to observe the features of hybrid nanofluid as a coolant agent. At the same time, Devi and Devi [38],[39] focused on the numerical inspection of hybrid Cu-Al_2O_3/H_2O nanofluid flow and heat transfer augmentation over a stretching sheet. Waini et al. [40] examined the heat transfer characteristics of hybrid nanofluid past a nonlinear permeable stretching/shrinking surface, whereas Zainal et al. [41] explored the unsteady MHD flow of non-axisymmetric Homann stagnation point in three-dimensional Al_2O_3-Cu/water and a research on the stagnation point flow throughout a heated moving sheet towards hybrid nanofluid can be traced in [42]. The analysis of solution stability past an exponential surface in a hybrid nanofluid in the presence of suction/injection parameter have been carried out by Anuar et al. [43] meanwhile, Waini et al. [44] investigated the rate of heat transfer in hybrid nanofluid generated by an exponentially shrinking surface.

In a wide range of viable demands and applications from the industry, essential temperature alterations around the surrounding fluid and the surface does exist. These require the deliberation of heat generation or absorption on the temperature-dependent that could possibly develop an essential effect on the characteristic of heat transfer [45]. The appearance and implication of heat generation/absorption upon the boundary layer flow inquiry continue to be of considerable interest, mainly because of its various applications within the field of engineering systems, such as thermal insulation, cooling of atomic reactors, geothermal supplies, and others [46]. Vajravelu and Hadjinicolaou [47] analysed the boundary layer flow and heat transfer past a stretching sheet

in the presence of internal heat source, followed by [48], who expanded the effort of [47] by involving the radiation and viscosity effect. Naramgari and Sulochana [49] managed to obtain the non-uniqueness solutions of magnetic nanofluid flow with heat generation/absorption over an exponentially stretching sheet, whilst Megahed [50] scrutinised the thermal radiation and heat source impact through an exponentially porous stretching sheet inclusive of constant heat flux in a Newtonian fluid.

A closer look to the literature on the above-mentioned earlier, however, reveals a number of gaps and shortcomings. To our knowledge, no prior studies have examined the hybrid nanofluid flow past a bidirectional exponential stretching/shrinking sheet with the inclusion of the heat generation/absorption and MHD in their research framework. Thus, motivated by the above knowledge gap, our ultimate goal of this paper is to perform a numerical analysis of the heat generation/absorption impact towards a bidirectional exponential stretching/shrinking sheet on MHD flow in hybrid Al_2O_3-Cu/H_2O nanofluid. Besides, the current study utilised the bvp4c approach in MATLAB operating system (Matlab R2019b, MathWorks, Natick, Massachusetts, USA) in order to gain the problem solutions. There are several solutions to be anticipated; thus, the evaluation of solution stability is executed to confirm the solutions steadiness with an actual physical interpretation. This crucial contribution may help to improving industrial production, especially in the manufacturing and process sectors.

2. Mathematical model

Consider the steady three-dimensional MHD flow of a hybrid Al_2O_3-Cu/H_2O nanofluid over bidirectional exponential stretching/shrinking sheet with heat generation/absorption effect in the plane $z=0$ and $x, y=0$ set at the origin O, as displayed in Fig. 1. We assume that the surface

temperature experienced at the wall differs exponentially in the form of $T_w(x,y) = T_\infty + T_0 e^{a(x+y)/2L}$ where T_∞ and T_0 are surrounding fluid temperature and reference temperature, respectively, while a denotes the parameter of exponent temperature. The velocity stretched uniformly, which governed by a bidirectional exponentially form with $u_w = ce^{\frac{x+y}{L}}$ in $x-$ axis and $v_w = de^{\frac{x+y}{L}}$ in $y-$ axis. At this point, L represents the distinctive length while c and d are the velocity references. The transverse magnetic field $B(x,y) = B_0 e^{\frac{x+y}{2L}}$ is time-dependant and reflected normal towards the stretching/shrinking sheet, where B_0 refer to the applied magnetic field strength. Since we assume the magnetic Reynolds number is minimal, hence the induced magnetic field can be neglected. Along with the Boussinesq approximations and Bernoulli's equation in the free stream, the hybrid Al_2O_3-Cu/H_2O nanofluid governing equations are identified as:

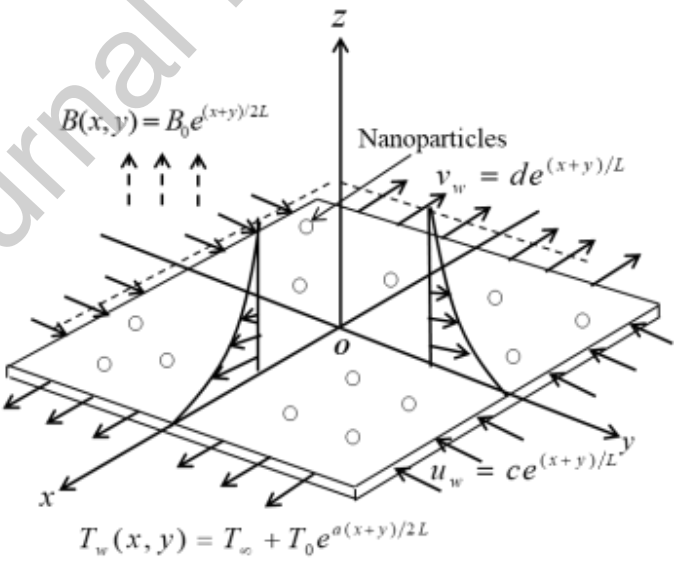

Fig. 1 The schematic of problem flow

$$\frac{\partial u}{\partial x}+\frac{\partial v}{\partial y}+\frac{\partial w}{\partial z}=0, \tag{1}$$

$$u\frac{\partial u}{\partial x}+v\frac{\partial u}{\partial y}+w\frac{\partial u}{\partial z}=\frac{\mu_{hnf}}{\rho_{hnf}}\frac{\partial^2 u}{\partial^2 z}-\frac{\sigma_{hnf}}{\rho_{hnf}}B^2u, \tag{2}$$

$$u\frac{\partial v}{\partial x}+v\frac{\partial v}{\partial y}+w\frac{\partial v}{\partial z}=\frac{\mu_{hnf}}{\rho_{hnf}}\frac{\partial^2 v}{\partial^2 z}-\frac{\sigma_{hnf}}{\rho_{hnf}}B^2v, \tag{3}$$

$$u\frac{\partial T}{\partial x}+v\frac{\partial T}{\partial y}+w\frac{\partial T}{\partial z}=\frac{k_{hnf}}{\left(\rho C_p\right)_{hnf}}\frac{\partial^2 T}{\partial z^2}+\frac{Q}{\rho C_p}\left(T-T_\infty\right), \tag{4}$$

subject to the boundary conditions:

$$\begin{aligned} &u=u_w\left(x\right),\ v=v_w\left(y\right),\ w=w_w\left(x,y\right)=w_0e^{\frac{x+y}{2L}},\ T=T_w,\\ &u\to 0, v\to 0, T\to T_\infty \text{ as } z\to\infty, \end{aligned} \tag{5}$$

provided that u is the velocity component along the $x-$ direction, while v and w denote the velocity towards $y-$ and $z-$ directions, respectively, w_0 is a constant, T implies the Al_2O_3-Cu/H_2O temperature, μ_{hnf} is the Al_2O_3-Cu/H_2O dynamic viscosity, ρ_{hnf} the Al_2O_3-Cu/H_2O density, k_{hnf} is the Al_2O_3-Cu/H_2O thermal conductivity, $\left(\rho C_p\right)_{hnf}$ is the Al_2O_3-Cu/H_2O heat capacity, σ_{hnf} is the Al_2O_3-Cu/H_2O electrical conductivity, and Q is the heat generation/absorption coefficient. The Cu thermophysical properties, along with Al_2O_3 and H_2O, are exhibited in Table 1 [51]. Here, ϕ represents the nanoparticles volume fraction, ρ_f and ρ_s stand for the base fluid and hybrid nanoparticles densities, $\left(\rho C_p\right)_s$ and $\left(\rho C_p\right)_f$ are the hybrid nanoparticles heat capacity together with base fluid, C_p is the constant pressure of heat capacity, k_f is the thermal conductivity of the base fluid, and lastly the thermal conductivity of hybrid nanoparticles is indicated by k_s. On the other hand, Table 2 provides the hybrid Al_2O_3–Cu/H_2O nanofluids thermophysical properties, which has been constituted in [37].

Table 1 The Cu thermophysical properties along with Al_2O_3 and H_2O

Physical properties	Cu	Al_2O_3	H_2O
$k\left(\mathrm{W/mK}\right)$	400	40	0.613
$\rho\left(\mathrm{kg/m^3}\right)$	8933	3970	997.1
$C_p\left(\mathrm{J/kgK}\right)$	385	765	4179
$\beta\times10^{-5}\left(\mathrm{mK}\right)$	1.67	0.85	21

Table 2 Hybrid nanofluids thermophysical properties

Properties	Hybrid nanofluid
Dynamic viscosity	$\mu_{hnf}=\dfrac{1}{\left(1-\phi_{hnf}\right)^{2.5}}$
Density	$\rho_{hnf}=\left(1-\phi_{hnf}\right)\rho_f+\phi_1\rho_{s1}+\phi_2\rho_{s2}$
Thermal capacity	$\left(\rho C_p\right)_{hnf}=\left(1-\phi_{hnf}\right)\left(\rho C_p\right)_f+\phi_1\left(\rho C_p\right)_{s1}+\phi_2\left(\rho C_p\right)_{s2}$
Thermal conductivity	$\dfrac{k_{hnf}}{k_f}=\left[\dfrac{\left(\dfrac{\phi_1k_{s1}+\phi_2k_{s2}}{\phi_{hnf}}\right)+2k_f+2\left(\phi_1k_{s1}+\phi_2k_{s2}\right)-2\phi_{hnf}k_f}{\left(\dfrac{\phi_1k_{s1}+\phi_2k_{s2}}{\phi_{hnf}}\right)+2k_f-\left(\phi_1k_{s1}+\phi_2k_{s2}\right)+\phi_{hnf}k_f}\right]$
Electrical conductivity	$\dfrac{\sigma_{hnf}}{\sigma_f}=\left[\dfrac{\left(\dfrac{\phi_1\sigma_{s1}+\phi_2\sigma_{s2}}{\phi_{hnf}}\right)+2\sigma_f+2\left(\phi_1\sigma_{s1}+\phi_2\sigma_{s2}\right)-2\phi_{hnf}\sigma_f}{\left(\dfrac{\phi_1\sigma_{s1}+\phi_2\sigma_{s2}}{\phi_{hnf}}\right)+2\sigma_f-\left(\phi_1\sigma_{s1}+\phi_2\sigma_{s2}\right)+\phi_{hnf}\sigma_f}\right]$

Now, we introduced the following similarity transformations [52]:

$$u=ce^{\frac{x+y}{L}}f'(\eta),\ v=ce^{\frac{x+y}{L}}g'(\eta),\ w=-\sqrt{\frac{c\nu_f}{2L}}e^{\frac{x+y}{2L}}\left[f(\eta)+\eta f'(\eta)+g(\eta)+\eta g'(\eta)\right],$$
$$\theta(\eta)=\frac{T-T_\infty}{T_0e^{\frac{a(x+y)}{2L}}},\ Q=Q_0e^{\frac{x+y}{L}},\ \eta=z\sqrt{\frac{c}{2\nu_fL}}e^{\frac{x+y}{2L}}, \tag{6}$$

and

$$w_0 = -\sqrt{\frac{c\nu_f}{2L}}S. \tag{7}$$

Here, S indicates the parameter of constant mass flux where $S>0$ and $S<0$ are for suction and injection, respectively. Implying the similarity transformation (6) into Eqs. (2)−(4) along with the boundary conditions (5), a set of ordinary (similarity) differential equations can be perceived as following:

$$\frac{\mu_{hnf}/\mu_f}{\rho_{hnf}/\rho_f} f''' + (f+g) f'' - 2f'^2 - 2f'g' - \frac{\sigma_{hnf}/\sigma_f}{\rho_{hnf}/\rho_f} Mf' = 0, \tag{8}$$

$$\frac{\mu_{hnf}/\mu_f}{\rho_{hnf}/\rho_f} g''' + (f+g) g'' - 2g'^2 - 2f'g' - \frac{\sigma_{hnf}/\sigma_f}{\rho_{hnf}/\rho_f} Mg' = 0, \tag{9}$$

$$\frac{1}{\Pr}\frac{k_{hnf}/k_f}{(\rho C_p)_{hnf}/(\rho C_p)_f}\theta'' + (f+g)\theta' - a(f'+g')\theta + H\theta = 0, \tag{10}$$

in conjunction with:

$$\begin{aligned} &f(0)=S,\ g(0)=0,\ f'(0)=1,\ g'(0)=\lambda,\ \theta(0)=1, \\ &f'(\eta)\to 0, g'(\eta)\to 0, \theta(\eta)\to 0 \text{ as } \eta\to\infty, \end{aligned} \tag{11}$$

where λ address the stretching/shrinking parameter($\lambda<0$ for shrinking, $\lambda>0$ for stretching), Pr represents the Prandtl number, H and M are the heat generation/absorption and the magnetic coefficient, respectively, which are described as follows:

$$\Pr = \frac{\nu_f}{\alpha_f},\ M = \frac{2L\sigma_f B_0^2}{c\rho_f},\ H = \frac{2LQ_0}{c\rho C_P},\ \lambda = \frac{d}{c},\ S = -\frac{w_0}{\sqrt{c\upsilon_f/2L}}. \tag{12}$$

The coefficient of skin friction C_{fx}, C_{fy} and the local Nusselt number Nu_x are the physical quantities of interest, which are defined as:

$$C_{fx} = \frac{\tau_w}{\rho_f u_w^{\ 2}},\ C_{fy} = \frac{\tau_w}{\rho_f v_w^{\ 2}},\ Nu_x = \frac{Lq_w}{k_f(T_w - T_\infty)}, \tag{13}$$

given that τ_{wx}, τ_{wy} connote the shear stress of the surface in the $x-$ and $y-$ axes, whilst q_w represents the heat flux, where:

$$\tau_{wx} = \mu_{hnf}\left(\frac{\partial u}{\partial z}\right)_{z=0}, \quad \tau_{wy} = \mu_{hnf}\left(\frac{\partial u}{\partial z}\right)_{z=0}, \; q_w = -k_{hnf}\left(\frac{\partial T}{\partial z}\right)_{y=0}. \tag{14}$$

By applying (6), (13) and (14), we get:

$$\left(2\,\mathrm{Re}_x\right)^{1/2} C_{fx} = \frac{\mu_{hnf}}{\mu_f} f''(0), \quad \left(2\lambda^3\,\mathrm{Re}_y\right)^{1/2} C_{fy} = \frac{\mu_{hnf}}{\mu_f} g''(0), \quad \left(\frac{2}{\mathrm{Re}_x}\right)^{1/2} \mathrm{Nu}_x = -\frac{k_{hnf}}{k_f}\theta'(0), \tag{15}$$

provided that $\mathrm{Re}_x = \dfrac{u_w L}{\nu_f}$ and $\mathrm{Re}_y = \dfrac{v_w L}{\nu_f}$, where Re_x and Re_y are the local Reynolds number in the $x-$ and $y-$ axes, correspondingly.

3. Analysis of solution stability

The numerical findings of Eqs. (8)–(11) imply the occurrence of non-uniqueness solutions for various values of selected parameters. There is a need to execute the stability analysis to confirm a dependable solution as first exposed by Merkin [53] and Merill et al. [54]. Now, we have:

$$\frac{\partial u}{\partial t} + u\frac{\partial u}{\partial x} + v\frac{\partial u}{\partial y} + w\frac{\partial u}{\partial z} = \frac{\mu_{hnf}}{\rho_{hnf}}\frac{\partial^2 u}{\partial^2 z} - \frac{\sigma_{hnf}}{\rho_{hnf}}B^2 u, \tag{16}$$

$$\frac{\partial u}{\partial t} + u\frac{\partial v}{\partial x} + v\frac{\partial v}{\partial y} + w\frac{\partial v}{\partial z} = \frac{\mu_{hnf}}{\rho_{hnf}}\frac{\partial^2 v}{\partial^2 z} - \frac{\sigma_{hnf}}{\rho_{hnf}}B^2 v, \tag{17}$$

$$\frac{\partial T}{\partial t} + u\frac{\partial T}{\partial x} + v\frac{\partial T}{\partial y} + w\frac{\partial T}{\partial z} = \frac{k_{hnf}}{\left(\rho C_p\right)_{hnf}}\frac{\partial^2 T}{\partial z^2} + \frac{Q}{\rho C_p}\left(T - T_\infty\right), \tag{18}$$

where τ is initiated to the problem as a time variable. Thus, we obtain:

$$u = ce^{\frac{x+y}{L}}\frac{\partial f(\eta,\tau)}{\partial \eta},\ v = ce^{\frac{x+y}{L}}\frac{\partial g(\eta,\tau)}{\partial \eta},$$
$$w = -\sqrt{\frac{c\nu_f}{2L}}e^{\frac{x+y}{2L}}\left(\begin{array}{c} f(\eta,\tau)+\eta\frac{\partial f(\eta,\tau)}{\partial \eta}+g(\eta,\tau)+\eta\frac{\partial g(\eta,\tau)}{\partial \eta} \\ +2\tau\frac{\partial f(\eta,\tau)}{\partial \tau}+2\tau\frac{\partial g(\eta,\tau)}{\partial \tau}\end{array}\right), \tag{19}$$
$$\theta(\eta,\tau) = \frac{T-T_\infty}{T_0 e^{\frac{a(x+y)}{2L}}},\ \eta = z\sqrt{\frac{c}{2\nu_f L}}e^{\frac{x+y}{2L}},\ \tau = \frac{ct}{2L}e^{\frac{x+y}{L}}.$$

Consequently, we substitute (19) into Eqs. (16), (17) and (18) the resulting system of equations is produced:

$$\frac{\mu_{hnf}/\mu_f}{\rho_{hnf}/\rho_f}\frac{\partial^3 f}{\partial \eta^3}+(f+g)\frac{\partial^2 f}{\partial \eta^2}-2\left(\frac{\partial f}{\partial \eta}+\frac{\partial g}{\partial \eta}\right)\frac{\partial f}{\partial \eta}-\frac{\sigma_{hnf}/\sigma_f}{\rho_{hnf}/\rho_f}M\frac{\partial f}{\partial \eta}-\frac{\partial^2 f}{\partial \eta \partial \tau}=0, \tag{20}$$

$$\frac{\mu_{hnf}/\mu_f}{\rho_{hnf}/\rho_f}\frac{\partial^3 g}{\partial \eta^3}+(f+g)\frac{\partial^2 g}{\partial \eta^2}-2\left(\frac{\partial f}{\partial \eta}+\frac{\partial g}{\partial \eta}\right)\frac{\partial g}{\partial \eta}-\frac{\sigma_{hnf}/\sigma_f}{\rho_{hnf}/\rho_f}M\frac{\partial g}{\partial \eta}-\frac{\partial^2 g}{\partial \eta \partial \tau}=0, \tag{21}$$

$$\frac{1}{\Pr}\frac{k_{hnf}/k_f}{(\rho C_p)_{hnf}/(\rho C_p)_f}\frac{\partial^2 \theta}{\partial \eta^2}+(f+g)\frac{\partial \theta}{\partial \eta}-a\left(\frac{\partial f}{\partial \eta}+\frac{\partial g}{\partial \eta}\right)\theta+H\theta-\frac{\partial \theta}{\partial \tau}=0, \tag{22}$$

agree with the following boundary conditions:

$$\begin{aligned} &f(0,\tau)=S,\ g(0,\tau)=0,\ \frac{\partial f}{\partial \eta}(0,\tau)=1,\ \frac{\partial g}{\partial \eta}(0,\tau)=\lambda,\ \theta(0,\tau)=1, \\ &\frac{\partial f}{\partial \eta}(\eta,\tau)\to 0,\frac{\partial g}{\partial \eta}(\eta,\tau)\to 0,\theta(\eta,\tau)\to 0 \text{ as } \eta\to\infty. \end{aligned} \tag{23}$$

To analyse the steady flow solution stability $f(\eta)=f_0(\eta), g(\eta)=g_0(\eta)$ and $\theta(\eta)=\theta_0(\eta)$, we write [55]:

$$\begin{aligned} f(\eta,\tau) &= f_0(\eta)+e^{-\omega\tau}F(\eta), \\ g(\eta,\tau) &= g_0(\eta)+e^{-\omega\tau}G(\eta), \\ \theta(\eta,\tau) &= \theta_0(\eta)+e^{-\omega\tau}I(\eta), \end{aligned} \tag{24}$$

where ω is an unknown parameter of the eigenvalue and functions $F(\eta), G(\eta)$ and $I(\eta)$ are relatively small to $f_0(\eta), g_0(\eta)$ and $\theta_0(\eta)$. Now, we substitute Eq. (24) into Eqs. (20)–(22) together with (23), we get:

$$\frac{\mu_{hnf}/\mu_f}{\rho_{hnf}/\rho_f}\frac{\partial^3 F}{\partial \eta^3}+(f_0+g_0)\frac{\partial^2 F}{\partial \eta^2}+(F+G)\frac{\partial^2 f_0}{\partial \eta^2}-2\left(\frac{\partial f_0}{\partial \eta}+\frac{\partial g_0}{\partial \eta}\right)\frac{\partial F}{\partial \eta}-2\left(\frac{\partial F}{\partial \eta}+\frac{\partial G}{\partial \eta}\right)\frac{\partial f_0}{\partial \eta} -\frac{\sigma_{hnf}/\sigma_f}{\rho_{hnf}/\rho_f}M\frac{\partial F}{\partial \eta}+\omega\frac{\partial F}{\partial \eta}=0, \tag{25}$$

$$\frac{\mu_{hnf}/\mu_f}{\rho_{hnf}/\rho_f}\frac{\partial^3 G}{\partial \eta^3}+(f_0+g_0)\frac{\partial^2 G}{\partial \eta^2}+(F+G)\frac{\partial^2 g_0}{\partial \eta^2}-2\left(\frac{\partial f_0}{\partial \eta}+\frac{\partial g_0}{\partial \eta}\right)\frac{\partial G}{\partial \eta}-2\left(\frac{\partial F}{\partial \eta}+\frac{\partial G}{\partial \eta}\right)\frac{\partial g_0}{\partial \eta} -\frac{\sigma_{hnf}/\sigma_f}{\rho_{hnf}/\rho_f}M\frac{\partial G}{\partial \eta}+\omega\frac{\partial G}{\partial \eta}=0, \tag{26}$$

$$\frac{1}{\Pr}\frac{k_{hnf}/k_f}{(\rho C_p)_{hnf}/(\rho C_p)_f}\frac{\partial^2 I}{\partial \eta^2}+(F+G)\frac{\partial \theta_0}{\partial \eta}+(f_0+g_0)\frac{\partial I}{\partial \eta} -a\left(\frac{\partial f_0}{\partial \eta}+\frac{\partial g_0}{\partial \eta}\right)I-a\left(\frac{\partial F}{\partial \eta}+\frac{\partial G}{\partial \eta}\right)\theta_0-HI+\omega I=0, \tag{27}$$

$$F(0,\tau)=0,\ \mathrm{G}(0,\tau)=0,\ \frac{\partial F}{\partial \eta}(0,\tau)=0,\ \ \frac{\partial G}{\partial \eta}(0,\tau)=0,\ I(0,\tau)=0, \quad \frac{\partial F}{\partial \eta}(\eta,\tau)\to 0, \frac{\partial G}{\partial \eta}(\eta,\tau)\to 0, I(\eta,\tau)\to 0 \text{ as } \eta\to\infty. \tag{28}$$

The steady-state flow stability along with the solutions of heat transfer $f_0(\eta), g_0(\eta)$ and $\theta_0(\eta)$ is analysed by fixing $\tau\to 0$. Subsequently, the early development or solution decay of (24) is possible to assess. Hence, the corresponding linearised eigenvalue problem is defined:

$$\frac{\mu_{hnf}/\mu_f}{\rho_{hnf}/\rho_f}F'''+(f_0+g_0)F''+(F+G)f_0''-2\left(f_0'+g_0'\right)F'-2(F'+G')f_0' -\frac{\sigma_{hnf}/\sigma_f}{\rho_{hnf}/\rho_f}MF'+\omega F'=0, \tag{29}$$

$$\frac{\mu_{hnf}/\mu_f}{\rho_{hnf}/\rho_f}G''' + (f_0 + g_0)G'' + (F+G)g_0'' - 2\left(f_0' + g_0'\right)G' - 2(F'+G')g_0' - \frac{\sigma_{hnf}/\sigma_f}{\rho_{hnf}/\rho_f}MG' + \omega G' = 0, \tag{30}$$

$$\frac{1}{\Pr}\frac{k_{hnf}/k_f}{(\rho C_p)_{hnf}/(\rho C_p)_f}I'' + (F+G)\theta_0' + (f_0+g_0)I' - a\left(\left(f_0' + g_0'\right)I + (F'+G')\theta_0\right) - HI + \omega I = 0, \tag{31}$$

subject to:

$$F(0)=0,\ G(0)=0,\ F'(0)=0,\ G'(0)=0,\ I(0)=0,\quad F'(\eta)\to 0,\ G'(\eta)\to 0, I(\eta)\to 0 \text{ as } \eta\to\infty. \tag{32}$$

As projected by [56], the possible series of ω could be computed by resting the boundary condition on $F'(0)$, $G'(0)$ or $I(\eta)$. In the current work, by normalising $F''(0)=1$ while relaxing $F'(\eta)\to 0$, the value of ω is possible to acquire by finding the solutions of the linearised eigenvalue problem as in Eqs. (29)–(31), along with boundary conditions (32). The result of the smallest eigenvalues ω_1 is capable of indicating the stability of flow solutions in $f_0(\eta), g_0(\eta)$ and $\theta_0(\eta)$. The positive smallest eigenvalue signifies the solution stability where there exists an initial decay of disturbances as time develops gradually while the negative value suggests a rise in disturbances, and therefore, the flow is unreliable.

4. Results and discussion

In order to obtain the numerical results of this study, the system of ordinary differential equations (8)–(11) were solved by using a built-in function that comes with the MATLAB operating system, known as bvp4c [57]. The bvp4c adaptive solver modified the mesh points at

each step in the iterative process, assigning them to points where they are most desired. Thus, it is essential to prepare a starting assumption within the starting point of the mesh, advantageous to the exactness of the required solution. This excellent solver has contributed to the visible benefits in terms of storage and computational costs, hence enabling control over the grid resolution. Besides, it has been broadly operated by numerous analysts to tackle the boundary value issue because of its capability on generating non-uniqueness solutions. Even so, the average processor time for computing the outcomes can vary relying upon the use of the initial guesses. A sample code on solving the system of ordinary differential equations (8) – (11) coded in the bvp4c solver can be accessed in Appendix 1.

The hybrid $Al_2O_3 - Cu/H_2O$ nanofluid is endorsed in this current work with a different range of ϕ values. It is essential to mention that in the remarkable study of Turkyilmazoglu [58], he stated that the resulting nanofluid tends to behave like a non-Newtonian fluid when the nanoparticles volumetric concentration surpasses 5% to 6%. Thus, in this study, copper and alumina nanoparticles volume fraction is specified in between $0.02 \le \phi \le 0.04$, corresponds to the work of [58]. Devi and Devi [38],[59], reported that the hybrid $Al_2O_3 - Cu/H_2O$ nanofluid is established by dispersing Al_2O_3 nanoparticles (ϕ_1) into H_2O followed by Cu as the second nanoparticle (ϕ_2) with acceptable amounts of solid nanoparticles volume fractions. It should be pointed out that the dispersion of single nanoparticle (Al_2O_3/Cu) is qualified to produce $Al_2O_3 - H_2O$ and $Cu - H_2O$ nanofluid. Since the current work is consistent with the water-based nanofluid, the Prandtl number is set to 6.2 along the analysis execution of this study, excluding similarities with the preceding argument. The numerical findings are confirmed with Jusoh et al. [22] who employed the bvp4c function in their outstanding work, and Ahmad et al. [60] utilised

a standard fifth-order Runge-Kutta approach combined with the shooting method, as disclosed in Table 3.

It is found that the current results are in a high consensus with past discoveries despite the different approaches of boundary value problem solver. Thus, we are confident that the reported mathematical model is suitable for exploring the heat transfer features and boundary layer flow of the current problem and is reasonable to use in practice.

Table 3 Comparison values of $\theta'(0)$ for several Pr, a and λ

λ	Pr	a	Present Result	Jusoh et al.[22]	Ahmad et al.[60]
0.0	0.7	–2.0	0.623618369	0.623618388	0.62363160
		0.0	–0.425838057	–0.425838050	–0.42583680
		2.0	–1.021436175	–1.021443621	–1.02143600
	7.0	–2.0	5.940944482	5.940943625	5.94098100
		0.0	–1.846605696	–1.846605768	–1.84660700
		2.0	–3.908918878	–3.908918599	–3.90891900
0.5	0.7	–2.0	0.763784546	0.763784494	0.76378700
		0.0	–0.521541039	–0.521541039	–0.52165550
		2.0	–1.250998201	–1.250998242	–1.25102600
	7.0	–2.0	7.276141279	7.276142356	7.27610600
		0.0	–2.261620849	–2.261622116	–2.26162200
		2.0	–4.787428350	–4.787442759	–4.78742800
1.0	0.7	–2.0	0.881943143	0.881943113	0.88196220
		0.0	–0.602223592	–0.602223595	–0.60222490
		2.0	–1.444528261	–1.444528306	–1.44452800
	7.0	–2.0	8.401764264	8.401765312	8.40172100
		0.0	–2.611494811	–2.611495069	–2.61150000
		2.0	–5.528046094	–5.528044818	–5.52804600

The presence of dual solutions was observed in the results obtained from Eqs. (8)–(10) respect to the boundary condition (11) for both stretching/shrinking case scenarios within a specified range of λ_c where λ_c denotes the dual solutions critical point known as the first and second solution. A unique solution is revealed when $\lambda = \lambda_c$ and no solutions exist when

$\lambda < \lambda_c$. The dual solutions appearance directs to an analysis of solution stability to decide a physically relevant solution. It is appeal highlighting that the first solution is presumed as a substantially reliable outcome and appears in practice. Figures $2-4$ exemplify the impacts of the nanoparticle volume fraction ϕ of $f''(0), g''(0)$ and $-\theta'(0)$ when $\phi_1(\text{alumina})$ is set to 0.02 and $\phi_2(\text{copper})$ vary in several values $(\phi_2 = 0.00, 0.02, 0.04)$. Observably, the results show that the increment in ϕ_2 escalates the values of $f''(0)$ and $g''(0)$ in both $Al_2O_3 - H_2O$ nanofluid $(\phi_2 = 0)$ and hybrid $Al_2O_3 - Cu/H_2O$ nanofluid $(\phi_2 = 0.02, 0.04)$ towards the stretching/shrinking sheet. This is due to the fact that increasing the volume fraction of nanoparticles boosts the fluid viscosity, which helped to improve the coefficient of skin friction through the surface. Moreover, Figs. 2 and 3 also convey that the rise of ϕ_2 enhances the values of $f''(0)$ and $g''(0)$ when the sheet is shrinking. Figure 4 shows the heat transfer characteristic pattern or $-\theta'(0)$ is reduced as there is an increase in the nanoparticle volume fraction in both ordinary fluid and hybrid nanofluid. In essence, the temperature of the sheet is amplified as the mass of the nanoparticles enlarges, hence the efficiency of thermal conductivity decreases and consequently affects the heat transfer rate of the working fluid. This may occur as a consequence of the internal heat generation influences that increased the temperature throughout the surface and disrupted the interaction of the nanoparticles, which then decrease the thermal conductivities.

Figures $5-7$ depict the magnetic parameter M influences towards $f''(0), g''(0)$ and $-\theta'(0)$ when $\phi_1 = \phi_2 = 0.02,$ which represents the hybrid $Al_2O_3 - Cu/H_2O$ nanofluid compound. In Figs. $5-6$, $f''(0)$ and $g''(0)$ increase as M increases because of the

reverse force, namely Lorentz force. This force appears to diminish the fluid velocity as a result of resistance against the motion of the fluid particles. The synchronisation of an electrical and magnetic field arising owing to the creation of Lorentz force appears to delay fluid progress. The boundary layer is getting thinner when M upsurges because of the adjourned flow, thus resulting in an augmentation of $f''(0)$ and $g''(0)$. The opposite trend was found in Fig. 7, which showed a declining pattern of $-\theta'(0)$ as M escalates. As reported before, the presence of the heat generation parameter H, has the tendency to increase the fluid thermal state and temperature distribution near the surface. The increment of the fluid temperature triggers more induced flow to the surface, allowing the thermal boundary layer thickness to enlarge hence, subsequently, decreasing the rate of heat transfer at the stretching/shrinking surface.

The rate of heat transfers also driven by the suction parameter (S), which is one of the concerned parameters in this study. Figures 8 – 10 portray the effects of the suction parameter on the velocity profiles in both x, y directions $\left(f''(0), g''(0)\right)$ and the heat transfer rate $-\theta'(0)$. Notably, Figs. 8 – 9 interpret the values of $f''(0)$ and $g''(0)$ enlarge when the suction parameter is available. The suction impact at the boundary decelerates the motion of nanofluid and amplifies the velocity gradient along the permeable stretching/shrinking surface. The suction emergence initiates the heated fluid movements approaching the wall, hence decelerate the buoyancy strengths caused by the sturdy viscosity impact, thus forming an unexpected velocity gradient. Next, Fig. 10 signifies the values of $-\theta'(0)$ which demonstrates an increase in the heat transfer rate when S was exposed along the stretching/shrinking surface. In general, as the magnitude of S intensifies, the heat transfer rate is improved correspondingly. The suction

parameter value's increments diminished the thickness of the thermal boundary layer, thereby increasing the temperature gradient at the surface.

By considering the heat generation parameter in the case study, the variation of $-\theta'(0)$ towards λ with specific values of a is depicted in Fig. 11. As the parameter of the temperature exponent rises in the hybrid nanofluid, the heat transfer rate decreases in the first solution, and an inverse pattern is observed in the other solution whereby an increasing trend in the heat transfer rate is reflected a higher value of a. The range of $-\theta'(0)$ is rising with a for $\lambda > -1$, while $-\theta'(0)$ is declined with the development of the temperature exponent parameter for $\lambda < -1$. However, the critical values of the different usage of a suggest no substantial impact on the magnitude of $-\theta'(0)$ and the heat transfer rate also achieved the equilibrium state at $\lambda = -1$ since we identified that the value of $-\theta'(0)$ are equal for all values of a. Figure 12 exposes the temperature profile distribution $\theta(\eta)$ with various values of a. The temperature profile shifts far from the wall when the values of a is increase. This indicates that the expanding effect becomes noticeable, and the thickness of the thermal boundary layer becomes thickened for higher values of a.

Figures 13 depicts the heat generation/absorption (H) impact towards $-\theta'(0)$ while Fig. 14 flaunts the temperature profile $\theta(\eta)$ of a hybrid nanofluid with the influences of H. From Fig 13, we noted that $-\theta'(0)$ is declined as the heat generation/absorption values are increased along the stretching/shrinking surface with $H = -1.0, -0.5, 0.0, 0.5, 1.0$. Additionally, Fig. 14 shows the profile of dimensionless temperature $\theta(\eta)$ and it is evident that the temperature distribution spikes when the heat generation occurs and the temperature is deteriorated in regard

to the heat absorption parameter. The main reason for this phenomenon is because of the extra energy that produced in the boundary layer due to the presence of the heat generation $(\lambda = 3)$ in the fluid, which subsequently proliferates the thickness of the thermal boundary layer associated with the temperature, resulting from the buoyancy effect. Meanwhile, the amount of energy is observed in the event of heat absorption $(\lambda = -3)$, known as cooling of the fluid, whereby decreased the flow velocity of the boundary layer. In conclusion, the thermal state of the fluid increases due to the existence of a heat generation effect hence triggers the thermal boundary layer to lift. If the heat generation intensity is relatively high, the maximum fluid temperature does not occur at the wall, but rather in the surrounding fluid region. On another note, the appearance of the impact of heat absorption causes the thermal condition of the fluid to decrease, thereby creating lower thermal boundary layers, as proven in Fig. 14.

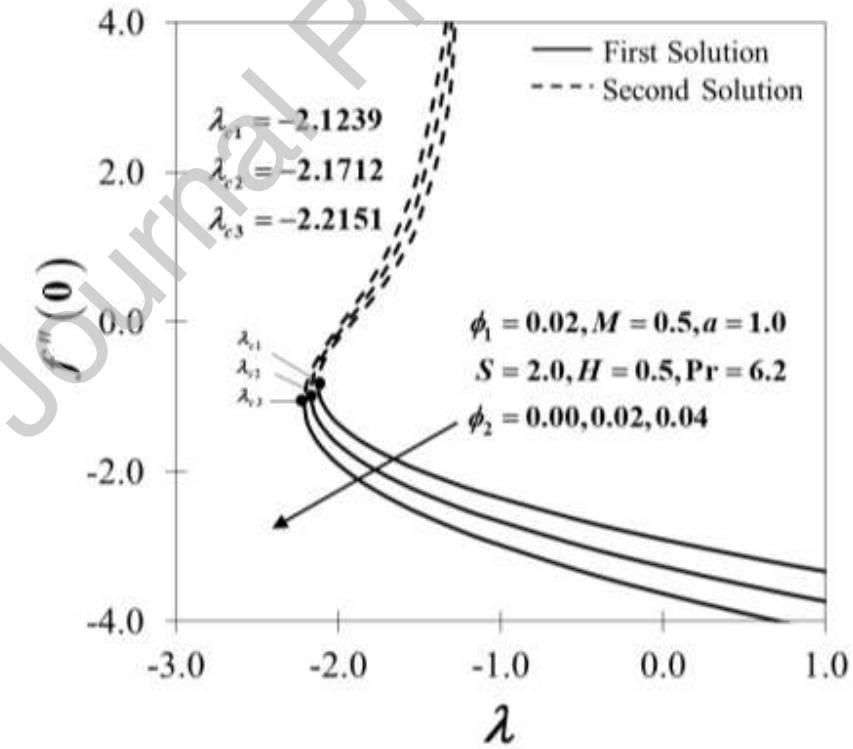

Fig. 2 Variants of $f''(0)$ towards λ with $\phi_2 = 0.00, 0.02, 0.04$

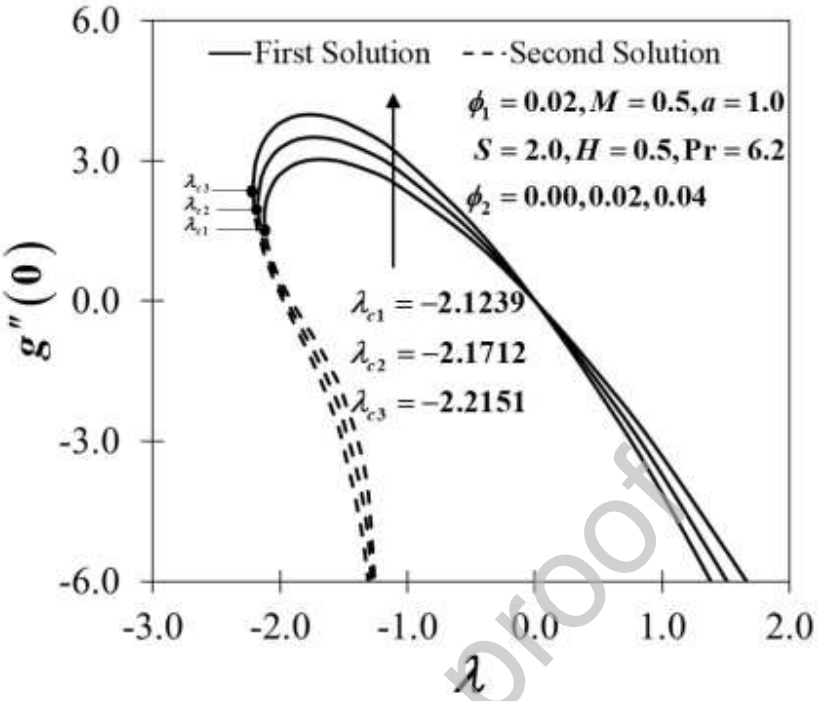

Fig. 3 Variants of $g''(0)$ towards λ with $\phi_2 = 0.00, 0.02, 0.04$

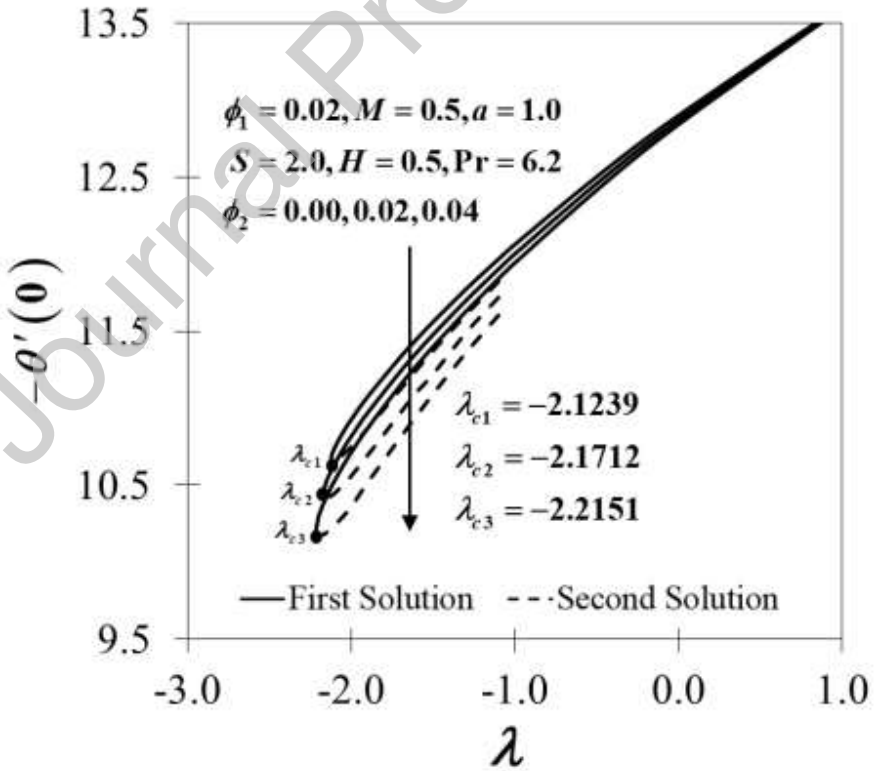

Fig. 4 Variants of $-\theta'(0)$ towards λ with $\phi_2 = 0.00, 0.02, 0.04$

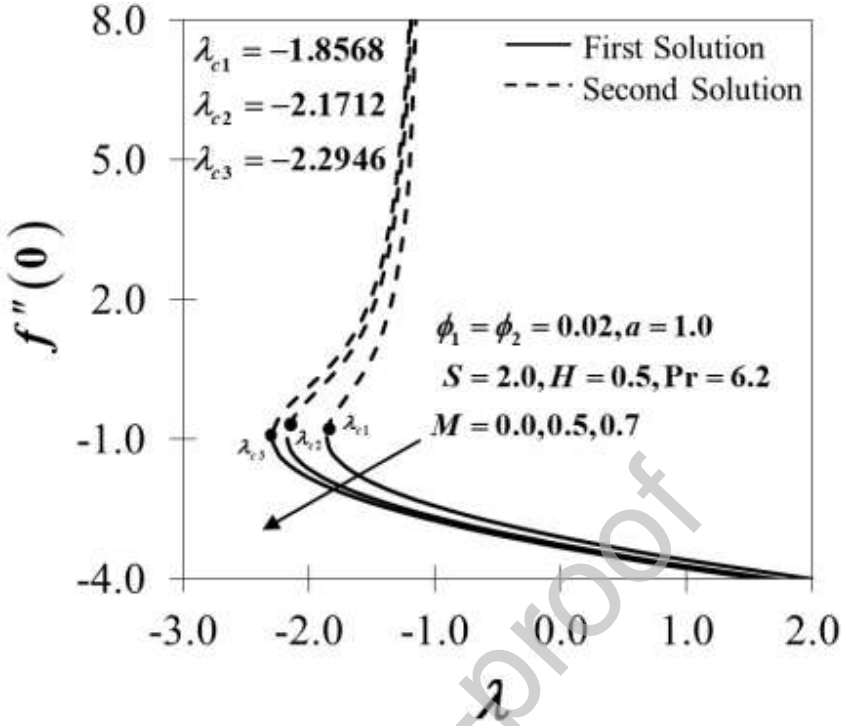

Fig. 5 Variants of $f''(0)$ towards λ with $M = 0.0, 0.5, 0.7$

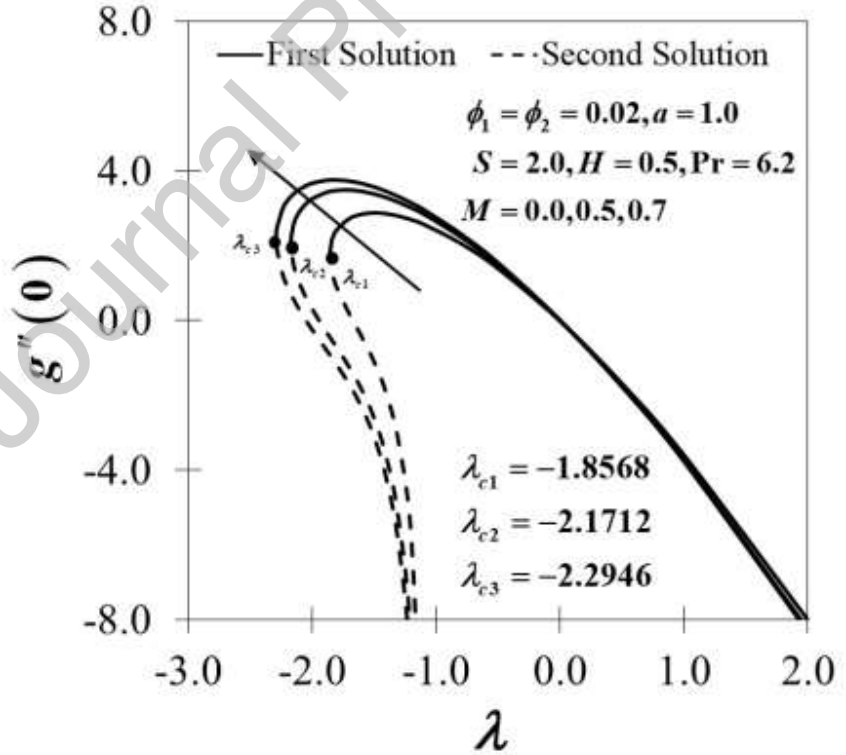

Fig. 6 Variants of $g''(0)$ towards λ with $M = 0.0, 0.5, 0.7$

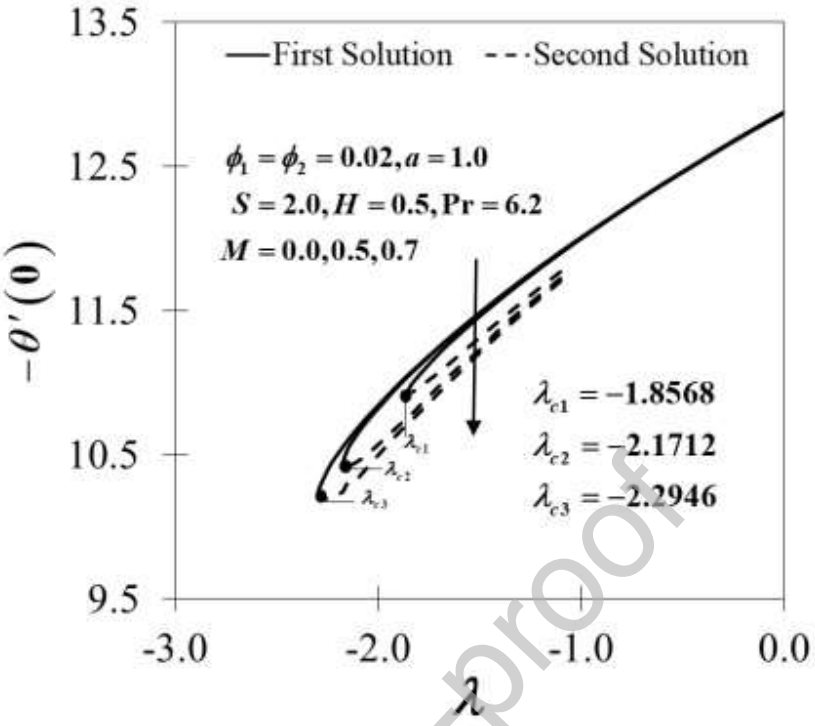

Fig. 7 Variants of $-\theta'(0)$ towards λ with $M = 0.0, 0.5, 0.7$

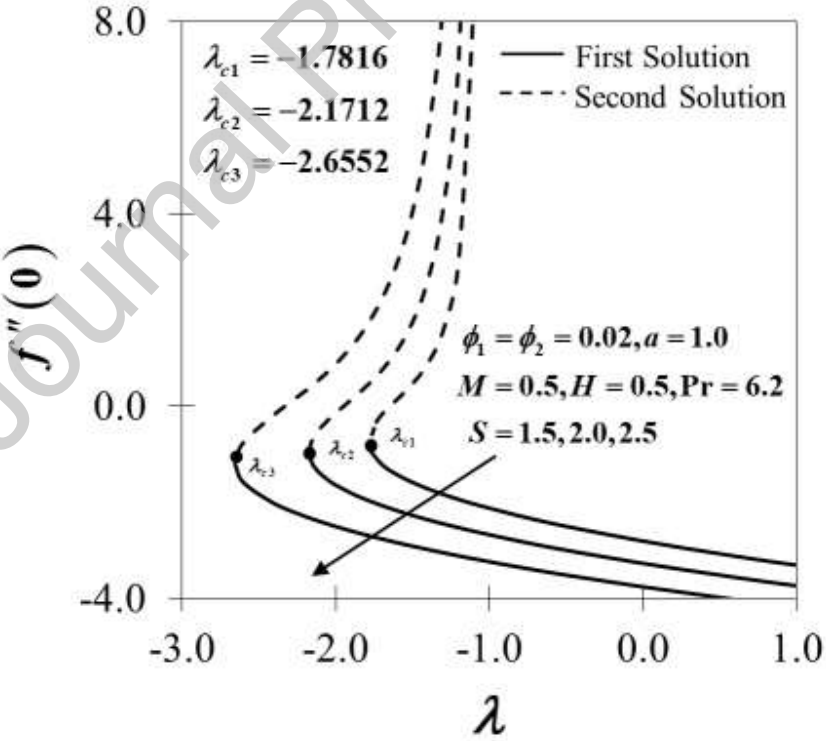

Fig. 8 Variants of $f''(0)$ towards λ with $S = 1.5, 2.0, 2.5$

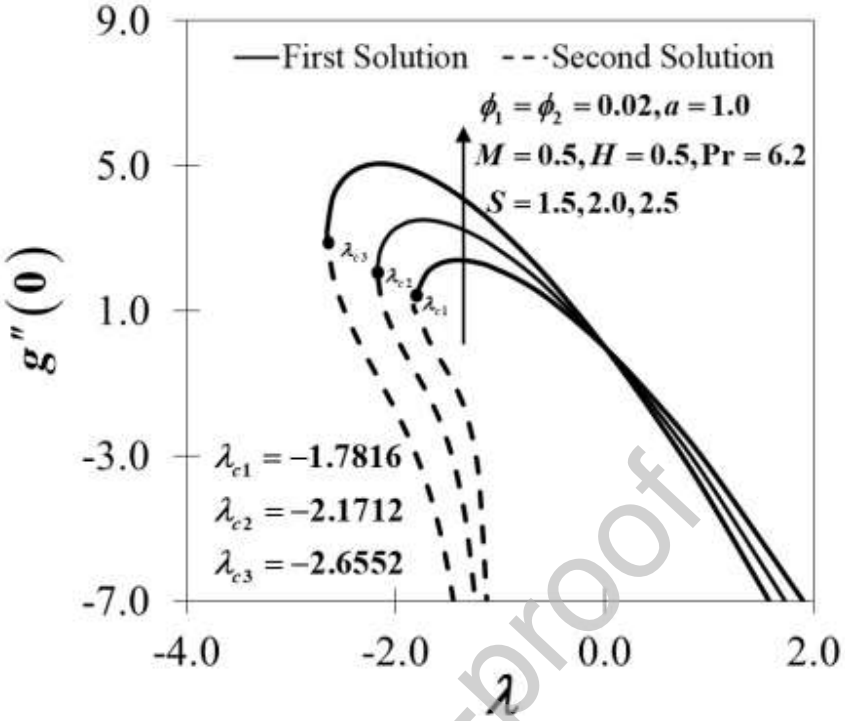

Fig. 9 Variants of $g''(0)$ towards λ with $S = 1.5, 2.0, 2.5$

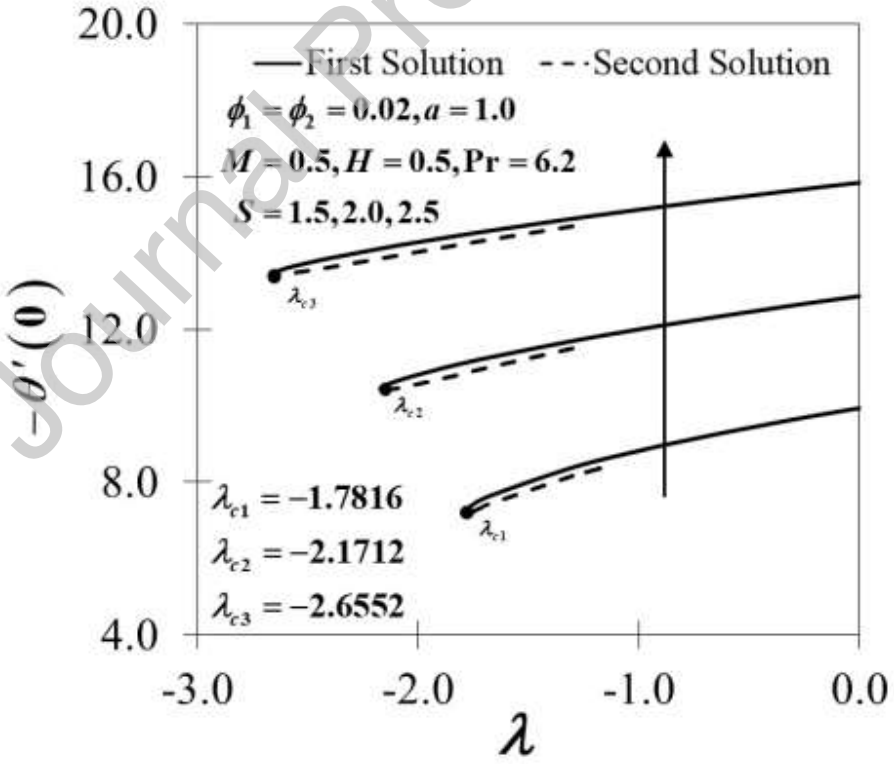

Fig. 10 Variants of $-\theta'(0)$ towards λ with $S = 1.5, 2.0, 2.5$

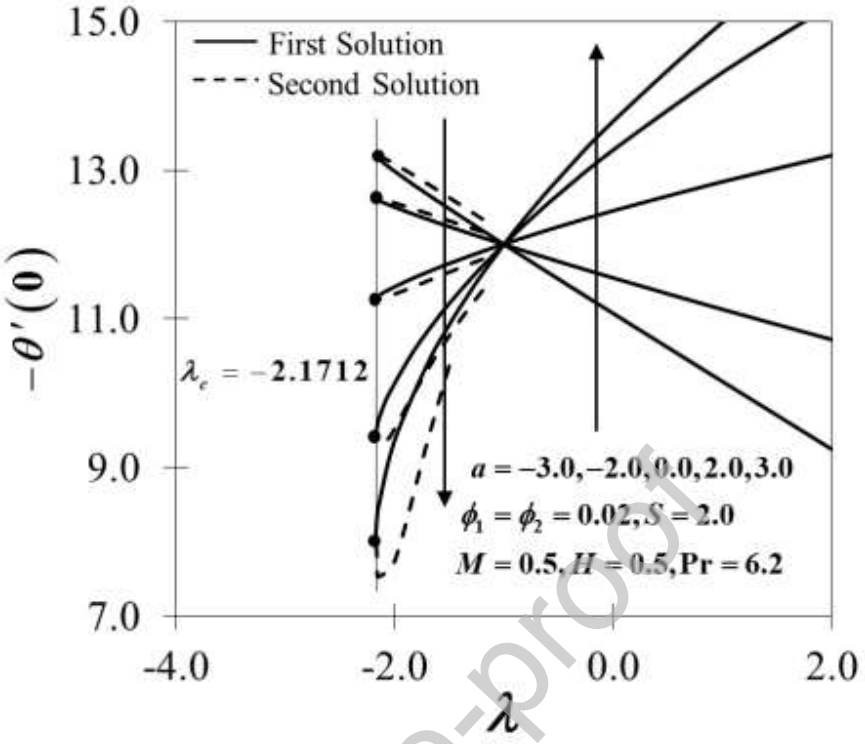

Fig. 11 Variants of $-\theta'(0)$ towards λ with $a = -3.0, -2.0, 0.0, 2.0, 3.0$

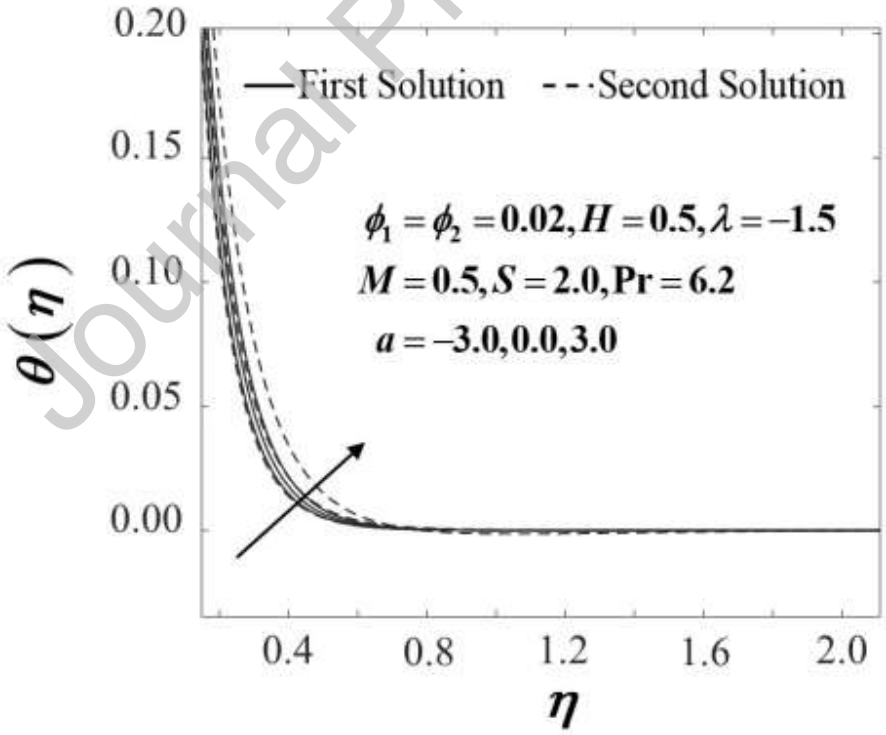

Fig. 12 Temperature profile of $\theta(\eta)$ towards η with $a = -3.0, -2.0, 0.0, 2.0, 3.0$

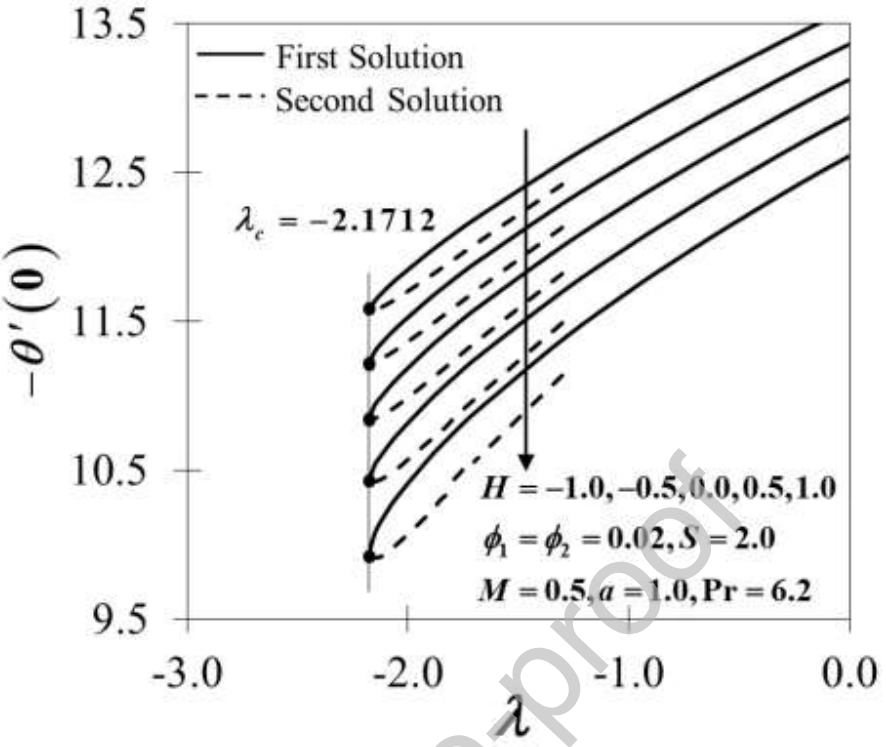

Fig. 13 Variants of $-\theta'(0)$ towards λ with $H = -1.0, -0.5, 0.0, 0.5, 1.0$

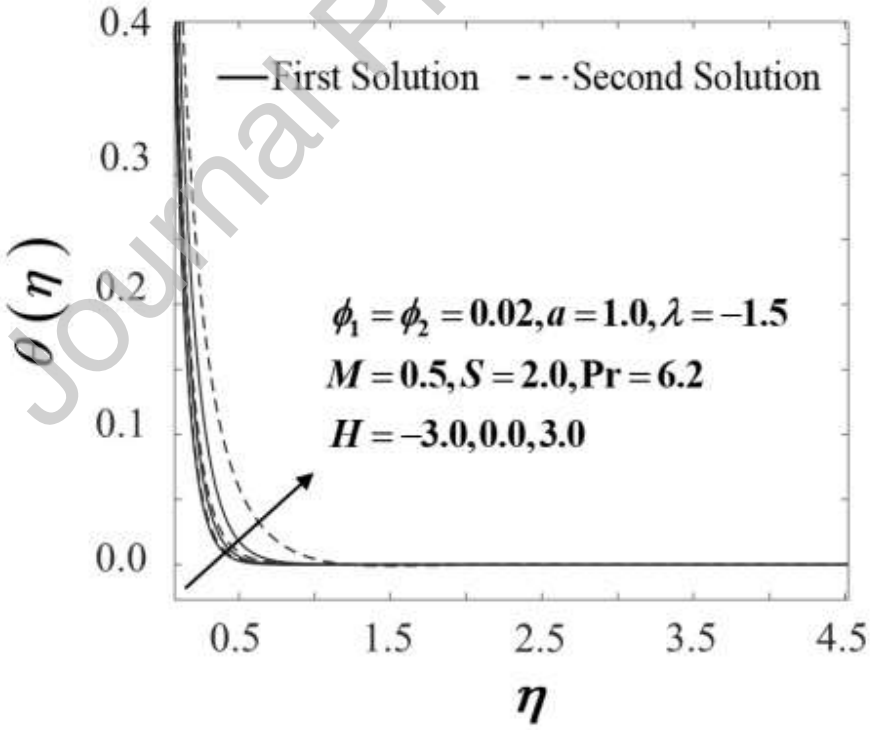

Fig. 14 Temperature profile of $\theta(\eta)$ towards η with $H = -1.0, -0.5, 0.0, 0.5, 1.0$

Since the findings contain a non-uniqueness solution, the stability analysis is carried out by utilising the bvp4c function that has been developed in MATLAB programming system to ensure the achievability of the generated results. If the smallest eigenvalue ω_1 is negative, the flow is considered unstable owing to the occurrence of disturbances in the early growth, whereas a positive value of the lowest eigenvalue reported a contrary consequence, which implies the physically attainable flow movement, where an initial deterioration of disturbance occurred. Table 4 establishes the smallest eigenvalue ω_1, which approximating to zero in either first or second solution while ω_1 reach λ_c. The positive value of ω_1 from the first solution described that the flow is stable and attainable.

Table 4 The smallest eigenvalues ω_1 of hybrid nanofluid when $M = 0.7$, $S = 2$, $\mathrm{H} = 0.5$, $a = 1.0$

λ	First solution (ω_1)	Second solution (ω_1)
-2	0.8666	-0.8451
-2.1	0.5851	-0.5744
-2.12	0.5005	-0.4926
-2.14	0.3942	-0.3892
-2.16	0.2391	-0.2372
-2.165	0.1793	-0.1783
-2.171	0.0445	-0.0444
-2.1712	0.0312	-0.0311

5. Conclusions

This work was designed to scrutinise the heat transfer features and boundary layer characteristics on magnetohydrodynamics (MHD) hybrid nanofluid $(\mathrm{Al_2O_3 - Cu/H_2O})$ over bidirectional exponential stretching/shrinking sheet by considering the heat generation/absorption impact. By adopting an effective transformation of the similarities

variable, the ordinary differential equations system was achieved through a simplification of governing partial differential equations. Our discoveries appear to conclude that there exist non-uniqueness solutions in the hybrid Al_2O_3-Cu/H_2O nanofluid over a broad range of stretching/shrinking parameters in both cases of assisting and opposing flows, whereby the boundary layer separation takes place in the regime of the opposing flow. The inclusion of the nanoparticle volume fraction and the magnetic parameter in the hybrid Al_2O_3-Cu/H_2O nanofluid decreased the local Nusselt number $-\theta'(0)$, however, at the same time improved both the skin friction coefficient $f''(0)$ and $g''(0)$, while an increase in the intensity of the suction parameter upsurges the heat transfer rate. In contrast, the appearance of heat generation boosts the thermal state of the hybrid nanofluid and consequently reduced the rate of heat transfer performance, whereas the inclusion of heat absorption parameter in the case study appears to help improving the heat transfer rate. Further, as the parameter of the temperature exponent rises, the hybrid Al_2O_3-Cu/H_2O nanofluid heat transfer rate is decreased. Since the dual solutions exist, the analysis of solution stability has confirmed the steadiness and constancy of the first solution, whereas the second solution is unstable and inconsistent.

Acknowledgements

The present work is endorsed by the research award (GUP-2019-034) from UKM, and all authors value the productive feedbacks by the competent reviewers.

Declaration of competing interest

The authors declare that there is no conflict of interest.

References

[1] Y.S. Daniel, Z.A. Aziz, Z. Ismail, F. Salah, Thermal radiation on unsteady electrical MHD

flow of nanofluid over stretching sheet with chemical reaction, J. King Saud Univ-Sci. 31 (2017) 804–812.

[2] R. Van Gorder, K. Vajravelu, Multiple solutions for hydromagnetic flow of a second grade fluid over a stretching or shrinking sheet, Q. Appl. Math. 69 (2011) 405–424.

[3] K.B. Pavlov, Magnetohydrodynamic flow of an incompressible viscous fluid caused by deformation of a plane surface, Magn. Gidrodin. 4 (1974) 146–147.

[4] H.S. Takhar, M. Ali, A.S. Gupta, Stability of magnetohydrodynamic flow over a stretching sheet, Mech. Fluids Transp. Process. 10 (1989) 465–471.

[5] M. Hashemi-Tilehnoee, A.S. Dogonchi, S.M. Seyyedi, A.J. Chamkha, D.D. Ganji, Magnetohydrodynamic natural convection and entropy generation analyses inside a nanofluid-filled incinerator-shaped porous cavity with wavy heater block, J. Therm. Anal. Calorim. 141 (2020) 2033–2045.

[6] A.S. Dogonchi, M. Waqas, S.R. Afshar, S.M. Seyyedi, M. Hashemi-Tilehnoee, A.J. Chamkha, D.D. Ganji, Investigation of magneto-hydrodynamic fluid squeezed between two parallel disks by considering Joule heating, thermal radiation, and adding different nanoparticles, Int. J. Numer. Methods Heat Fluid Flow 30 (2019) 659–680.

[7] A.S. Dogonchi, A.J. Chamkha, M. Hashemi-Tilehnoee, S.M. Seyyedi, D.D. Ganji, Effects of homogeneous-heterogeneous reactions and thermal radiation on magneto-hydrodynamic Cu-water nanofluid flow over an expanding flat plate with non-uniform heat source, J. Cent. South Univ. 26 (2019). 1161–1171.

[8] A.S. Dogonchi, T. Tayebi, A.J. Chamkha, D.D. Ganji, Natural convection analysis in a square enclosure with a wavy circular heater under magnetic field and nanoparticles, J. Therm. Anal. Calorim. 139 (2020) 661–671.

[9] T. Altan, S. Oh, H. Gegel, M. Park, Metal Forming: Theory and Applications, American Society of Metals, Metals Park 1983.

[10] E.G. Fisher, Extrusion of Plastics. Wiley, New York, 1976.

[11] M.V. Karwe Y. Jaluria, Numerical simulation of thermal transport associated with a continuously moving flat sheet in materials processing, J. Heat Transfer. 113 (1991) 612–619.

[12] B.C. Sakiadis, Boundary-layer behavior on continuous solid surfaces: I. Boundary-layer equations for two-dimensional and axisymmetric flow, AIChE J. 7 (1961) 26–28.

[13] L.J. Crane, Flow past a stretching plate, J. Appl. Math. Phys. 21 (1970) 645–647.

[14] E. Magyari, B. Keller, Heat and mass transfer in the boundary layers on an exponentially stretching continuous surface, J. Phys. D. Appl. Phys. 32 (1999) 577.

[15] M. Sajid, T. Hayat, Influence of thermal radiation on the boundary layer flow due to an exponentially stretching sheet, Int. Commun. Heat Mass Transf. 35 (2008) 347–356.

[16] M.A. El-Aziz, Viscous dissipation effect on mixed convection flow of a micropolar fluid over an exponentially stretching sheet, Can. J. Phys. 87 (2009) 359–368.

[17] S. Mukhopadhyay, Slip effects on MHD boundary layer flow over an exponentially stretching sheet with suction/blowing and thermal radiation, Ain Shams Eng. J. 4 (2013) 485–491.

[18] S. Nadeem, R. Ul Haq, Z.H. Khan, "Heat transfer analysis of water-based nanofluid over an exponentially stretching sheet, Alexandria Eng. J. 53 (2014) 219–224.

[19] M. Miklavčič, C.Y. Wang, Viscous flow due to a shrinking sheet, Q. Appl. Math. 64, (2006) 283–290.

[20] K. Bhattacharyya, Boundary layer flow and heat transfer over an exponentially shrinking

sheet, Chinese Phys. Lett. 28 (2011) 074701.

[21] E.H. Hafidzuddin, R. Nazar, N.M. Arifin, I. Pop, Boundary layer flow and heat transfer over a permeable exponentially stretching/shrinking sheet with generalised slip velocity, J. Appl. Fluid Mech. 9 (2016) 2025–2036.

[22] R. Jusoh, R. Nazar, I. Pop, Magnetohydrodynamic boundary layer flow and heat transfer of nanofluids past a bidirectional exponential permeable stretching/shrinking sheet with viscous dissipation effect, J. Heat Transf. 141 (2019) 012406.

[23] L.A. Lund, Z. Omar, I. Khan, Quadruple solutions of mixed convection flow of magnetohydrodynamic nanofluid over exponentially vertical shrinking and stretching surfaces: Stability analysis, Comput. Methods Programs Biomed. 182 (2019) 105044.

[24] S. Dero, A.M. Rohni, A. Saaban, MHD micropolar nanofluid flow over an exponentially stretching/shrinking surface: Triple solutions, J. Adv. Res. Fluid Mech. Therm. Sci. 56 (2019) 165–174.

[25] I. Waini, A. Ishak, I. Pop, Unsteady flow and heat transfer past a stretching/shrinking sheet in a hybrid nanofluid, Int. J. Heat Mass Transf. 136 (2019) 288–297.

[26] S.U. Choi, J. Eastman, Enhancing thermal conductivity of fluids with nanoparticles, ASME Publ. Fed. 231 (1995) 99–103.

[27] R.K. Tiwari, M.K. Das, Heat transfer augmentation in a two-sided lid-driven differentially heated square cavity utilising nanofluids, Int. J. Heat Mass Transf. 50 (2007) 2002–2018.

[28] J. Buongiorno, Convective transport in nanofluids, J. Heat Transfer 128 (2006) 240–250.

[29] M. Molana, A.S. Dogonchi, T. Armaghani, A.J. Chamkha, D.D. Ganji, I. Tlili, Investigation of hydrothermal behavior of Fe_3O_4-H_2O nanofluid natural convection in a novel shape of porous cavity subjected to magnetic field dependent (MFD) viscosity, J.

Energy Storage 30 (2020) 101395.

[30] A.S. Dogonchi, M.K. Nayak, N. Karimi, A.J. Chamkha, D.D. Ganji, Numerical simulation of hydrothermal features of Cu–H_2O nanofluid natural convection within a porous annulus considering diverse configurations of heater, J. Therm. Anal. Calorim. 141 (2020) 2109–2125.

[31] S.M. Seyyedi, A.S. Dogonchi, M. Hashemi-Tilehnoee, D.D. Ganji, A.J. Chamkha, Second law analysis of magneto-natural convection in a nanofluid filled wavy-hexagonal porous enclosure, Int. J. Numer. Methods Heat Fluid Flow (2020). https://doi.org/10.1108/HFF-11-2019-0845.

[32] S. Mondal, A.S. Dogonchi, N. Tripathi, M. Waqas, S.M Seyyedi, M. Hashemi-Tilehnoee, D.D. Ganji, A theoretical nanofluid analysis exhibiting hydromagnetics characteristics employing CVFEM, J. Braz. Soc. Mech. Sci. Eng. 42 (2020) 1–12.

[33] I. Tlili, S.M. Seyyedi, A.S. Dogonchi, M. Hashemi-Tilehnoee, D.D. Ganji, Analysis of a single-phase natural circulation loop with hybrid-nanofluid, Int. Commun. Heat Mass Transf. 112 (2020) 104498.

[34] S. Suresh, K.P. Venkitaraj, P. Selvakumar, M. Chandrasekar, Effect of Al_2O_3-Cu/water hybrid nanofluid in heat transfer, Exp. Therm. Fluid Sci. 38 (2012) 54–60.

[35] C.J. Ho, J.B. Huang, P.S. Tsai, Y.M. Yang, On laminar convective cooling performance of hybrid water-based suspensions of Al_2O_3 nanoparticles and MEPCM particles in a circular tube, Int. J. Heat Mass Transf. 54 (2011) 2397–2407.

[36] R. Nasrin, M.A. Alim, Finite element simulation of forced convection in a flat plate solar collector: Influence of nanofluid with double nanoparticles, J. Appl. Fluid Mech. 7 (2014) 543–556.

[37] D. Madhesh, S. Kalaiselvam, Experimental analysis of hybrid nanofluid as a coolant, Procedia Eng. 97 (2014) 1667–1675.

[38] S.P.A. Devi, S.S.U. Devi, Numerical investigation of hydromagnetic hybrid Cu−Al_2O_3/water nanofluid flow over a permeable stretching sheet with suction, Int. J. Nonlinear Sci. Numer. Simul. 17 (2016) 249–257.

[39] S.U. Devi, S.P.A. Devi, Heat transfer enhancement of Cu−Al_2O_3/water hybrid nanofluid flow over a stretching sheet, J. Niger. Math. Soc. 36 (2017) 419–433.

[40] I. Waini, A. Ishak, I. Pop, Hybrid nanofluid flow and heat transfer over a nonlinear permeable stretching/shrinking surface, Int. J. Numer. Methods Heat Fluid Flow 29 (2019) 3110–3127.

[41] N.A. Zainal, R. Nazar, K. Naganthran, I. Pop, Unsteady three-dimensional MHD non-axisymmetric Homann stagnation point flow of a hybrid nanofluid with stability analysis, Mathematics 8 (2020) 784 (25 pages).

[42] N.A. Zainal, R. Nazar, K. Naganthran, I. Pop, MHD mixed convection stagnation point flow of a hybrid nanofluid past a vertical flat plate with convective boundary condition, Chin. J. Phys. 66 (2020) 630–644.

[43] N.S. Anuar, N. Bachok, N.M. Arifin, H. Rosali, Effect of suction/injection on stagnation point flow of hybrid nanofluid over an exponentially shrinking sheet with stability analysis, CDF Lett. 11 (2019) 21–33.

[44] I. Waini, A. Ishak, I. Pop, Hybrid nanofluid flow induced by an exponentially shrinking sheet, Chin. J. Phys. 68 (2020) 468-482.

[45] K. Vajravelu, J. Nayfeh, Hydromagnetic convection at a cone and a wedge, Int. Commun. Heat Mass Transf. 19 (1992) 701–710.

[46] P. Garg, G.N. Purohit, B. Vidyapeeth, R.C. Chaudhary, A similarity solution for laminar thermal boundary layer over a flat plate with internal heat generation and a convective surface boundary condition, J. Rajasthan Acad. Phys. Sci. 14 (2015) 221–226.

[47] K. Vajravelu, A. Hadjinicolaou, Heat transfer in a viscous fluid over a stretching sheet with viscous dissipation and internal heat generation, Int. Commun. Heat Mass Transf. 20 (1993) 417–430.

[48] E.M. Abo-Eldahab, M.S. El Gendy, Radiation effect on convective heat transfer in an electrically conducting fluid at a stretching surface with variable viscosity and uniform free stream, Phys. Scr. 62 (2000) 321–325.

[49] S. Naramgari, C. Sulochana, Dual solutions of radiative MHD nanofluid flow over an exponentially stretching sheet with heat generation/absorption, Appl. Nanosci. 6 (2016) 131–139.

[50] A.M. Megahed, Numerical solution for variable viscosity and internal heat generation effects on boundary layer flow over an exponentially stretching porous sheet with constant heat flux and thermal radiation, J. Mech. 30 (2014) 395–402.

[51] E. Abu-Nada, H.F. Oztop, Effects of inclination angle on natural convection in enclosures filled with Cu-water nanofluid, Int. J. Heat Fluid Flow 30 (4) (2009) 669–678.

[52] I.C. Liu, H.H. Wang, Y.F. Peng, Flow and heat transfer for three-dimensional flow over an exponentially stretching surface, Chem. Eng. Commun. 200 (2013) 253–268.

[53] J.H. Merkin, Mixed convection boundary layer flow on a vertical surface in a saturated porous medium, J. Eng. Math. 14 (1980) 301–313.

[54] K. Merrill, M. Beauchesne, J. Previte, J. Paullet, P. Weidman, Final steady flow near a stagnation point on a vertical surface in a porous medium, Int. J. Heat Mass Transf. 49

(2006) 4681–4686.

[55] P.D. Weidman, D.G. Kubitschek, A.M.J. Davis, The effect of transpiration on self-similar boundary layer flow over moving surfaces, Int. J. Eng. Sci. 44 (2006) 730–737.

[56] S.D. Harris, D.B. Ingham, I. Pop, Mixed convection boundary-layer flow near the stagnation point on a vertical surface in a porous medium: Brinkman model with slip, Transp. Porous Media 77 (2009) 267–285.

[57] L.F. Shampine, I. Gladwell, S. Thompson, Solving ODEs with Matlab, Cambridge University Press, 2003.

[58] M. Turkyilmazoglu, A note on the correspondence between certain nanofluid flows and standard fluid flows, J. Heat Transf. 137 (2015) 2014–2016.

[59] S.S.U. Devi, S.P.A. Devi, Numerical investigation of three-dimensional hybrid Cu–Al_2O_3/water nanofluid flow over a stretching sheet with effecting Lorentz force subject to Newtonian heating, Can. J. Phys. 94 (2016) 490–496.

[60] R. Ahmad, M. Mustafa, T. Hayat, A. Alsaedi, Numerical study of MHD nanofluid flow and heat transfer past a bidirectional exponentially stretching sheet, J. Magn. Magn. Mater. 407 (2016) 69–74.

Nomenclature

The following symbols and abbreviations are used in this manuscript:

Roman letters

a	exponent temperature parameter
Al_2O_3	alumina
c, d	constant $(-)$
B_0	applied magnetic field strength $(-)$
C_{fx}, C_{fy}	skin friction coefficient in the $x-$ and $y-$ directions $(-)$

C_p	specific heat at constant pressure $\left(\mathrm{Jkg^{-1}K^{-1}}\right)$
Cu	copper
H	heat generation/absorption parameter $(-)$
H_2O	water
k	thermal conductivity of the fluid $\left(\mathrm{Wm^{-1}K^{-1}}\right)$
L	distinctive length $(-)$
M	magnetic parameter $(-)$
Nu_x	local Nusselt number $(-)$
$\left(pC_p\right)$	heat capacitance of the fluid $\left(\mathrm{JK^{-1}m^{-3}}\right)$
Pr	Prandtl number $(-)$
Q	heat generation/absorption coefficient $(-)$
Q_0	initial value of the heat generation/absorption coefficient $(-)$
Re_x	local Reynolds number in $x-$ direction $(-)$
Re_y	local Reynolds number in $y-$ direction $(-)$
S	constant mass flux parameter $(-)$
t	time (s)
T_w	surface temperature (K)
T_∞	surrounding fluid temperature (K)
T_0	reference temperature (K)
u,v,w	velocities component in the x–, $y-$ and $z-$ directions $\left(\mathrm{ms^{-1}}\right)$
u_w	velocities of the stretching/shrinking surface in $x-$ direction $\left(\mathrm{ms^{-1}}\right)$
v_w	velocities of the stretching/shrinking surface in $y-$ direction $\left(\mathrm{ms^{-1}}\right)$
w_0	mass flux velocity $(-)$
x,y,z	Cartesian coordinates (m)

Greek symbols

η	similarity variable $(-)$
θ	dimensionless temperature $(-)$
λ	stretching/shrinking parameter $(-)$
μ	dynamic viscosity of the fluid $\left(\mathrm{kgm^{-1}s^{-1}}\right)$
ν	kinematic viscosity of the fluid $\left(\mathrm{m^2s^{-1}}\right)$
ρ	density of the fluid $\left(\mathrm{kgm^{-3}}\right)$

σ	electrical conductivity $(\mathrm{S/m})$
τ	dimensionless time variable $(-)$
τ_{wx}, τ_{wy}	wall shear stress in the $x-$ and $y-$ directions $\left(\mathrm{kgm^{-1}s^{-2}}\right)$
ϕ_1	nanoparticle volume fractions for Al_2O_3 (alumina) $(-)$
ϕ_2	nanoparticle volume fractions for Cu (copper) $(-)$
ω	eigenvalue $(-)$; and
ω_1	smallest eigenvalue $(-)$.

Subscripts

f	base fluid $(-)$
nf	nanofluid $(-)$
hnf	hybrid nanofluid $(-)$
$s1$	solid component for Al_2O_3 (alumina) $(-)$
$s2$	solid component for Cu (copper) $(-)$
w	condition at the surface $(-)$; and
∞	condition outside of the boundary layer $(-)$.

Superscript

'	differentiation with respect to η $(-)$.

Appendix 1

To solve the system of ordinary differential equations (8)−(10) with the boundary condition (11), it is necessary to simplify these equations as follows:

$$f = y1, \quad f' = y2, \quad f'' = y3,$$
$$g = y4, \quad g' = y5, \quad g'' = y6,$$
$$\theta = y7, \quad \theta' = y5,$$
$$f''' = -\frac{\rho_{hnf}/\rho_f}{\mu_{hnf}/\mu_f}\left((f+g)f'' - 2f'^2 - 2f'g' - \frac{\sigma_{hnf}/\sigma_f}{\rho_{hnf}/\rho_f}Mf'\right),$$
$$= -\frac{\rho_{hnf}/\rho_f}{\mu_{hnf}/\mu_f}\left((y1+y4)y3 - 2(y2)^2 - 2(y2)(y5) - \frac{\sigma_{hnf}/\sigma_f}{\rho_{hnf}/\rho_f}M(y2)\right),$$
$$g''' = -\frac{\rho_{hnf}/\rho_f}{\mu_{hnf}/\mu_f}\left((y1+y4)y6 - 2(y5)^2 - 2(y2)(y5) - \frac{\sigma_{hnf}/\sigma_f}{\rho_{hnf}/\rho_f}M(y5)\right),$$

subject to:

$$ya1 - S, \quad ya2 - 1, \quad ya4, \quad ya5 - \lambda, \quad ya7 - 1,$$
$$yb2, \quad yb5, \quad yb7,$$

where *ya* and *yb* denotes the initial and far field conditions, respectively.

The solver syntax, sol = bvp4c(@OdeBVP,@OdeBc,solinit,options) includes the function handle @OdeBVP, into which the Eqs. (8)−(10) are coded. The boundary conditions (11) are then coded into the function handle @OdeBC.